A model and measurement comparison of diurnal cycles of sun-induced chlorophyll fluorescence of crops

Christiaan van der Tol[a,*], Micol Rossini[b], Sergio Cogliati[b], Wouter Verhoef[a], Roberto Colombo[b], Uwe Rascher[c], Gina Mohammed[d]

[a] *University of Twente, Faculty of Geo-Information Science and Earth Observation (ITC), P.O. Box 217, 7500 AE Enschede, The Netherlands*
[b] *Remote Sensing of Environmental Dynamics Lab., DISAT, University of Milano - Bicocca, Plazza della Scienza 1, 20126 Milan, Italy*
[c] *Institute of Bio- and Geosciences, IBG-2: Plant Sciences, Forschungszentrum Jülich GmbH, Jülich, Germany*
[d] *P&M Technologies, 66 Millwood Street, Sault Ste. Marie, Ontario, Canada*

Abstract

In this study, measurements of solar induced chlorophyll fluorescence (SIF) at 760 nm (F_{760}) are combined with hyperspectral reflectance (R) measurements collected in the field over agricultural crops in order to better understand the fluorescence (ChlF) signal of the vegetation. The 'Soil-Canopy Observation Photosynthesis and Energy fluxes' (SCOPE) model, which combines radiative transfer and enzyme kinetics of photosynthesis with turbulent heat exchange in vegetation canopies, was partly inverted to obtain model parameters from R taken over healthy (unstressed) crops during the growing season. Reflectance spectra between 400 and 900 nm obtained at midday on different days in the growing season were used to obtain pigment concentrations, leaf area index and leaf inclination. These parameters were then used to simulate diurnal cycles of half-hourly ChlF spectra, using measured weather variables as input. Three scenarios were simulated: (i) a constant emission efficiency of ChlF (at the photosystem level), (ii) a variable emission efficiency calculated per half hour with an electron transport, photosynthesis and ChlF model for the photosystem, and (iii) a constant emission efficiency that was set to a theoretical maximum value

*Corresponding author. Tel.:+31534874282
Email address: c.vandertol@utwente.nl (Christiaan van der Tol)

for fully blocked photochemical electron transport of photosytem II and minimal non-photochemical quenching. The simulations of the first two scenarios were compared to ChlF retrieved from field measurements in the O_2A band with the spectral fitting method in unstressed rice and alfalfa. This comparison and a sensitivity analysis showed that SCOPE reproduces most of the seasonal variability of SIF after tuning to R even if the ChlF emission efficiency is kept constant, and F_{760} values are mostly determined by chlorophyll content, dry matter, senescent material and leaf area and leaf inclination, whereas leaf water and carotenoid content had small effects. Diurnal variations in the ChlF emission efficiency at photosystem level were small in these crops. The simulations of the third scenario were compared to measurements of grass that was treated chemically to block electron transport and to provoke maximum ChlF. This comparison showed that the observed increase in F_{760} can indeed be explained by a change in the ChlF emission efficiency at the photosystem level. It is concluded that hyperspectral reflectance and the ChlF signal together can reveal both the dynamics of vegetation structure and functioning.

Keywords: chlorophyll fluorescence, radiative transfer model, spectroscopy, crop phenology

1. Introduction

The emerging data of airborne and satellite solar induced chlorophyll fluorescence (SIF) create opportunities for obtaining new information about vegetation status through remote sensing. SIF is the emission of energy in the red and far-red region of the electromagnetic spectrum by pigments that are involved in light harvest and photosynthetic electron transport in plants. Photochemical quenching was first mentioned as a cause of variability in chlorophyll fluorescence (ChlF) in the literature in the 19th century (Müller, 1874), and ChlF measurements in controlled conditions on algae and terrestrial plants have been undertaken for many years using both active and passive techniques (for reviews, see Baker (2008) and Meroni et al. (2009)). The Fraunhofer Line Discrimination

(FLD) method to decouple SIF from R of terrestrial vegetation was introduced by Plascyk (1975), but the possibility to apply this method at large area, from airborne or satellite platforms, is relatively new. The first papers presenting global satellite maps of SIF were published only a few years ago from data of GOSAT, GOME-2 and OCO-2 (Frankenberg et al., 2011; Joiner et al., 2011; Guanter et al., 2012; Joiner et al., 2013; Frankenberg et al., 2014). Retrievals of SIF from airborne sensors using medium spectral resolution non-imaging sensors (Damm et al., 2014) and high spectral and spatial resolution imaging sensors (Rascher et al., 2015) have been demonstrated recently as well. In addition, the Fluorescence Explorer satellite mission FLEX has been selected by the European Space Agency (ESA) as the 8th mission in the Earth Explorer series. FLEX will carry a hyperspectral instrument allowing SIF retrievals at different wavelengths in addition to hyperspectral reflectance, and it will be complemented with the optical and thermal bands of Sentinel-3 with which FLEX will fly in tandem.

It has been empirically demonstrated that SIF is a good indicator of photochemical activity in terrestrial vegetation (Damm et al., 2010), even better than indices based on reflectance (R) (Meroni et al., 2008a,b; Guanter et al., 2014). Indeed, there is evidence that SIF provides different information than reflectance spectra (Rossini et al., 2015), because SIF only originates from the parts of the vegetation that photosynthesize. This is further supported by the fact that SIF responds to a range of physiological stresses exerted on the vegetation (Ač et al., 2015).

A key aspect is how to best obtain useful information from SIF, and how to combine SIF and R data for better understanding of the vegetation status. ChlF depends on the actions of light harvesting pigments, the leaf area and leaf orientation, and the efficiencies of the ~~two~~ main de-excitation pathways of chlorophyll, notably photochemical quenching via electron transport (PQ) and thermal dissipation or non-photochemical quenching (NPQ) (Porcar-Castell et al., 2014). These ~~two~~ pathways compete with ChlF. Under low light, the excitation energy is efficiently used by photochemistry (PQ), while under high light exessive en-

ergy is dissipated as heat ~~via~~ by unregulated thermal dissipation and by various physiological NPQ mechanisms (Krause and Weis, 1991). The ChlF emission efficiency usually peaks between these extremes. SIF is thus always a function of both vegetation leaf (pigment) composition, leaf area and leaf inclination on the one hand, and the biochemical regulation of the energy pathways on the other hand. The vegetation architecture and pigment composition can be retrieved from the spectral signature, i.e., the shape of the reflectance curve as a function of wavelength over the solar reflective range (Jacquemoud et al., 2009). It is also possible to detect subtle variations in the reflectance due to changes in epoxidation state of the xanthophyll cycle related to NPQ (Garbulsky et al., 2011), and this can be detected from airborne data (Zarco-Tejada et al., 2012) and from space as well (Coops et al., 2010; Hilker et al., 2009; Drolet et al., 2008; Hall et al., 2008). SIF may therefore be partly explained by reflectance, but also provide complementary information to the rich signal of reflectance.

In several studies in the last years, the model 'Soil-Canopy Observation of Photosynthesis and Energy fluxes' (SCOPE) (Van der Tol et al., 2009) has been used to interpret SIF. SCOPE combines radiative transfer in the canopy with a Soil-Vegetation-Atmosphere Transfer (SVAT) scheme for the energy balance and photosynthesis. It contains routines for radiative transfer of solar radiation and radiation emitted by the vegetation (thermal and ChlF), and a routine for PQ and NPQ. SCOPE has been used to, for example, investigate the seasonality of SIF and productivity in parts of the Amazonia (Lee et al., 2013) and to retrieve the photosynthetic capacity of crops (Zhang et al., 2014). Even with a tool like the SCOPE model it is not easy to unravel the signal of SIF and to understand how it is related to processes and interactions within the vegetation. The model is complex and inevitably has representation errors due to model abstractions, and uncertainty in parameters and driving variables (in this paper we treat all vegetation properties as parameters, and all weather data as variables). Verrelst et al. (2015) addressed the problem of model complexity by carrying out a sensitivity analysis of SIF, as simulated by SCOPE, in order to identify the most sensitive model parameters and variables. It was shown that irradiance,

leaf composition, leaf area index and the carboxylation capacity V_{cmo} are the most influential parameters and variables affecting the signal of SIF. Most of the parameters and variables that affect SIF also influence reflectance. However, some, i.e., irradiance intensity, V_{cmo} and parameters for stomatal conductance, affect only SIF (not R), while others affect R rather strongly but have only a limited effect on SIF (leaf water content C_w). A practical question is thus, whether SCOPE can effectively explain the added value of SIF in understanding the functional status of vegetation. Up to now, a comparison between simulated SIF and field measurements of canopy ChlF has not been made in detail. ~~This aspect important:~~ To understand both simulated and observed diurnal and seasonal dynamics of ChlF is an important aspect. In this study we address this gap.

The objective of this investigation is therefore to utilize the SCOPE model to separately quantify the effects of leaf pigment concentrations and canopy architecture on SIF on the one hand, and the effects of PQ and NPQ on SIF on the other hand. We utilized existing datasets from published studies to obtain SCOPE parameter inputs. That work included measurements of reflectance in field crops using high-resolution (spatial, spectral) spectroscopy systems (Rossini et al., 2010; Cogliati et al., 2015a; Rossini et al., 2015). Parameter retrieval from R determined the value of most of the model parameters that affect SIF, notably the parameters of the PROSPECT (Jacquemoud and Baret, 1990) and SAIL (Verhoef, 1984) models. This enabled the simulation of SIF with SCOPE, then simulated SIF was compared to corresponding field measurements. In the comparison between model outputs and observations, we focused on diurnal cycles of several days in the growing season of rice and alfalfa crops. The selected days spanned different phenological stages, so that the effects of canopy density and greenness could be evaluated. The diurnal cycles enabled us to study the effects of PQ and NPQ, which vary during the day, while canopy density and greenness can be considered constant. Finally, data of a manipulation experiment, in which PQ was inhibited (Rossini et al., 2015), were used to further assess the effect of PQ on SIF.

2. Materials and methods

2.1. SCOPE model description

The SCOPE model (Van der Tol et al., 2009) consists of several routines that are combined to simulate ChlF. Since the first publication the model has undergone several revisions. For the present paper we used version 1.61 as published on https://github.com/Christiaanvandertol under GNU General Public Licence.

The illumination by direct solar light and diffuse sky light is simulated with the turbid medium model SAIL (Verhoef, 1984). The SAIL model calculates the scattering and absorption by leaves with a user-defined inclination distribution. Inputs of the SAIL model are the illumination above the canopy and the reflectance and transmittance of the leaves. The latter were originally calculated with the PROSPECT model, but in later versions (including version 1.61) PROSPECT has been replaced by the model Fluspect. The incident light is converted into emitted ChlF spectra on each side (top and bottom) of the leaf by Fluspect (Verhoef, 2011; Vilfan et al., submitted). This is done for all leaf layers and inclination classes. The emitted ChlF is finally used in a radiative transfer model to calculate top-of-canopy (TOC) SIF in the observation direction and hemispherically integrated. The canopy radiative transfer model for SIF is similar to SAIL, but it simulates the fate of emitted radiation rather than the incident radiation. Thus three aspects determine SIF in the SCOPE model: the distribution of light over leaves, the conversion of illumination into ChlF emission, and the propagation of ChlF through the canopy.

We now focus on the conversion of illumination into ChlF at the leaf level. The Fluspect model, which describes radiative transfer for a compact leaf, was used for this purpose. Fluspect is an extension of PROSPECT and includes the radiative transfer of ChlF (and re-absorption) within the leaf. The model uses an efficient doubling algorithm to solve the differential equations for radiative fluxes in the leaf mesophyll layer. It treats ChlF of the two photosystems, PSI and PSII, separately. The output of Fluspect (see Fig. 1) consists of leaf re-

flectance and transmittance as in PROSPECT and, in addition, the probability that excitation at a specific wavelength (λ_e) results in ChlF at a longer wavelength (λ_f) at the illuminated side (the backward direction) or at the shaded side (the forward direction). For λ_e, the spectral range from 400 to 700 nm is used, while for λ_f 640 to 850 nm is used, both with a spectral resolution of 1 nm. The components of the two photosystems that are responsible for fluorescence, PSI and PSII, are handled separately, such that there are four fluorescence excitation-emission probability matrices: one for each photosystem in the forward and the backward direction. The fluorescence emission of a leaf is the product of the probability matrices and the irradiance spectrum, as shown in Fig. 1 c,d,f,g.

The input parameters of the Fluspect model are the chlorophyll and carotenoid concentrations C_{ab} and C_{ca}, the dry matter and leaf water concentrations C_{dm} and C_w, the brown pigment concentration C_s, the mesophyll scattering parameter N, and the efficiencies of fluorescence emission at photosystem level. Specific optical properties, notably the absorption spectra of C_{ab}, C_{dm} etc., and the spectral shape of the fluorescence emissions of the two photosystems, PSI and PSII, are fixed parameters.

The emission efficiencies of PSI and PSII are known to vary with irradiance, leaf temperature and other factors, depending on the de-excitation pathways (PQ and NPQ) in the pigment bed of the photosystems (Weis and Berry, 1987; Krause and Weis, 1991). In SCOPE, a separate routine is used to predict how these efficiencies vary: the biochemical routine that also calculates leaf photosynthesis and transpiration. The fluorescence emission efficiency first increases and then decreases as photosynthesis moves from light limitation to light saturation (Fig. 1a.). The peak of fluorescence in this model appears to be 1.44 times the fluorescence efficiency at low light. Left of the peak (low light), most of the energy is dissipated through PQ, whereas right of the peak (high light), most of the excessive energy is dissipated through NPQ. The curve shown is empirically calibrated to data sets of PAM measurements on leaves of different species, but it may vary between species and sites depending on the complex

eco-physiological adaptation of photosynthesis in ways that are not fully understood.

In SCOPE, the biochemical routine is used to scale the fluorescence spectrum of PSII in response to the ambient environmental condition, relative to the efficiencies in unstressed, low light conditions, referred to as the F_o level in the literature (Maxwell and Johnson, 2000). The fluorescence emission spectra at the F_o-level were generated with Fluspect setting the efficiencies under F_o ~~for PSI and PSII~~ to 0.01 for PSII and 0.002 for PSI (Fig. 1c,f). The value for PSII was selected because (1) under low light, the ratio of the rate coefficients of photochemistry and PSII fluorescence is about 80:1, and (2) under low light about 80% of the photosynthetically active radiation is used for photochemistry (Van der Tol et al., 2014), thus 1% for fluorescence. The value for PSI and the spectral distributions of the emission by photosystems were derived from the study published by Franck et al. (2002).

Although SCOPE simulates the whole fluorescence spectrum, only the simulations at 760 nm have been used in this study, corresponding to the far red fluorescence as retrieved from the available field measurements.

2.2. Experimental data

SCOPE model performances were evaluated using two datasets of ~~top-of-canopy (TOC)~~ R and SIF collected in two crop fields equipped with meteorological and eddy covariance towers, and one collected over grass. These datasets cover different vegetation cases, with variability of structural and physiological parameters, which is suitable for modelling exercises.

The first dataset was collected in a rice (*Oryza sativa L.*) paddy field during seven field campaigns conducted in 2007 in Northern Italy (Rossini et al., 2010), but here only clear sky days are selected. The second consists of 27 consecutive days of measurements of R and SIF in an alfalfa (*Medicago sativa L.*) crop field in Central Italy (Cogliati et al., 2015a). Spectral data were collected manually in the rice field while the automatic Multiplexer Radiometer Irradiometer (MRI) system was employed for the alfalfa crop. Both measuring systems use

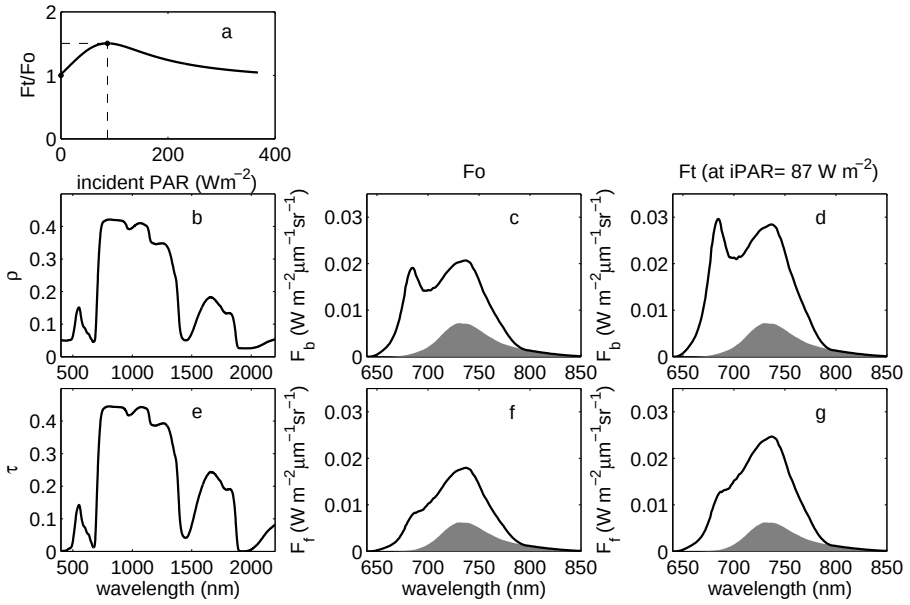

Figure 1: Example of the output of the combined Fluspect model and biochemical model: (a) simulation with the drought sensitive parameterization of the model of Van der Tol et al. (2014) of fluorescence emission efficiency F_t (a.u.) in the range 700-760 nm as a function of irradiance, normalized by the efficiency in low light conditions F_o. (b) Reflectance ρ and (e) transmittance τ simulated with the Fluspect model, and corresponding (c-d) backward (F_b) and (f-g) forward (F_f) fluorescence spectra normalized to total photosynthetically active irradiance (iPAR). The contribution by PSI is denoted by the gray area. Panels (c) and (f) are Fluspect simulations for the F_o-case, while in (d) and (g) the spectra of PSII represent the F_t-case at a PAR irradiance of 87 Wm^{-2}, corresponding to the peak in panel (a). The F_o-case only occurs at iPAR↓ 0, but for the sake of comparison to the F_t-case, it is shown for an irradiance of 87 Wm^{-2} as well. Note that the PSII spectrum is scaled such that integrated fluorescence is proportional to F_t/F_o in panel, while the PSI spectrum is unchanged (a). For these simulations, the Fluspect parameters of alfalfa of Julian day 164 (DOY = 164), and carboxylation capacity $V_{cmo} = 80$ μmol m^{-2} s^{-1} and Ball-Berry stomatal parameter $m = 10$ were used.

two portable spectrometers (HR4000, OceanOptics, USA) operating in the visible and near-infrared region but with different spectral resolutions. The first one covers the 400-900 nm spectral range with a full width at half maximum (FWHM) of 1 nm. The second one is optimized to provide higher spectral resolution (FWHM of 0.1 nm) in a restricted spectral range (700-800 nm) to estimate SIF in the O_2-A oxygen absorption band positioned at 760 nm (we use the symbol F_{760} for SIF in the O_2-A band in this study). Sun-induced fluorescence at 760 nm was estimated using the spectral fitting method (SFM) (Meroni et al., 2010), assuming a linear variation of reflectance and fluorescence in the O_2-A absorption band region. The spectral interval used for F_{760} estimation was set to 759.00 - 767.76 nm for a total of 439 spectral channels used. In the rice field, spectral data were acquired manually using bare fiber optics with an angular field of view of 25° using the method presented in Meroni et al. (2010). In the manual configuration, the rotation of a mast mounted horizontally on a tripod allowed alternative measurements of a white reference calibrated panel (Optopolymer GmbH, Germany) and the target. The MRI is developed for unattended operation and uses an upward pointing cosine receptor to measure irradiance and a bare fibre optic with an angular FOV of 25° to observe the target surface. The signal is divided by a computer-controlled multiplexer (MPM-2000, OceanOptics, USA). Spectrometers were spectrally and radiometrically calibrated with known standards (CAL-2000 mercury argon lamp and LS-1-CAL calibrated tungsten halogen lamp, OceanOptics, USA).

The third data set, acquired in the Czech Republic, consists of two days of data over two plots of lawn grass: a mixture consisting of *Festuca rubra*, *Lolium perenne* and *Poa pratensis*. One was a control plot and the other was treated with the herbicide DCMU (Dichorophenyl-dimethylurea) to experimentally block the linear photosynthetic electron flow at PSII (Rossini et al., 2015). In this experiment, the MRI system was used sequentially over the control and the treated plot. On the first measurement day, 5 September 2012, a relatively low concentration of DCMU was applied, whereas on the second measurement day (9 September 2012), a tenfold higher concentration was used. ~~These datasets~~

~~cover different vegetation cases, with variability of structural and physiological parameters, which is suitable for modelling exercises.~~

2.3. Parameter retrieval from reflectance

In Fig. 2 we show schematically how the model was applied. We first used Numerical Optimization (NO) for the retrieval of biophysical and biochemical parameters from apparent reflectance. We use the term 'apparent' reflectance because the measured reflectance is 'contaminated' by the fluorescence flux, i.e., TOC ~~the measured top-of-canopy (TOC)~~ radiance consists of reflected energy plus fluorescence. The retrieval was carried out using the optical radiative transfer routine of the SCOPE model code ('RTMo', where 'o' stands for 'optical'). One set of parameter values was retrieved separately for each of the measurement days, using the reflectance measured at midday, and next, SIF was simulated with the full SCOPE model using the retrieved parameters (a single set per day) and half-hourly weather data, as discussed in Section 2.4.

The general procedure for NO to retrieve parameters from apparent reflectance was as follows. The model was iteratively executed, each time with different parameter values, while aiming at minimizing a cost function. The cost function f was:

$$f = (R_s - R_m)^\top (R_s - R_m) + w \cdot (\frac{p - p_o}{\sigma_p})^\top (\frac{p - p_o}{\sigma_p}), \quad (1)$$

where R_s is the simulated and R_m the measured reflectance in all bands of the visible to near infrared (VNIR) spectra between 400 and 900nm, p the posterior and p_o the *a priori* values (also the initial values) of the parameters, σ_p is the assumed standard deviation of the *a priori* values of each parameter, and $w = 3 \cdot 10^{-3}$ is a weighting factor to scale the two parts of the cost function. The parameter w is necessary due to the different order of magnitude of the terms on the right hand side of Eq. (1), but the choice of its value w is subjective. The value chosen here ensures that the first part dominates the cost function. The second part only plays a role for the parameters to which the model is insensitive, and it prevents unrealistic posterior values for these parameters.

Similarly, the choice of *a priori* values and standard deviations is subjective, but again these values only affect model-insensitive parameters. We used the function 'lsqnonlin' of the optimization toolbox of Matlab R2013a, selecting a Trust Region algorithm for updating parameter values after each iteration step, and iteration stopped when the improvement of the cost function was less than a value of 10^{-3}. The ranges, initial values and standard deviations used are shown in Table 1.

Table 1: Lower boundaries (LB), upper boundaries (UB), *A priori* values (PV) and assumed standard deviations (σ_{p0}) of each parameter used for the retrieval. The first five parameters are Fluspect parameters for pigment content and leaf water content, followed by a transformation of the leaf area index LAI, the sum and the difference of the leaf inclination parameters $LIDFa$ and $LIDFb$, and four parameters (C_1 to C_4) that describe the shape of the fluorescence spectrum as a linear mixture four principle components.

Parameter	unit	LB	UB	PV	σ_{p0}
C_{ab}	μg cm^{-2}	0	100	40	30
C_{dm}	mg cm^{-2}	0	20	5	6
C_w	mg cm^{-2}	0	100	20	20
C_s	a.u.	0	0.4	0.1	0.2
C_{ca}	μg cm^{-2}	0	25	10	4
$1-\exp(-0.2LAI)$	m^{2}m^{-2}	0	0.7	0.45	0.2
$LIDFa+LIDFb$	-	-1	1	-0.5	0.6
$LIDFa-LIDFb$	-	-1	1	-0.2	0.6
C_1	-	0	40	0	∞
C_2	-	-20	20	0	∞
C_3	-	-10	10	0	∞
C_4	-	-2	2	0	∞

The following properties could potentially be retrieved from the apparent reflectance: (1) the leaf and canopy parameters of RTMo, (2) the soil (background) reflectance, and (3) the fluorescence spectrum. It appeared that only the leaf and canopy properties contributed substantially to the apparent reflectance.

For the soil background, we used the 'Global Soil Vector' (GSV) model (Verhoef et al., 2014), which simulates the soil spectrum as a linear combination of three basis spectra. In principle the parameters of the GSV model could be retrieved, but we found that for the crops in this study, the sensitivity of the simulated ~~top-of-canopy~~ TOC reflectance to the soil spectrum was negligible. For this reason, the parameters of the GSV model were fixed at 0.5, 25, 45 and 30 for the brightness, LAT and LON parameter and the soil moisture content, respectively. The measured apparent reflectance includes a small contribution from fluorescence, which was for some of the measurements visible as a spike in the spectra around 760 nm (i.e., in the O_2-A band). We corrected for this effect by adding a fluorescence spectrum on top of the radiance simulated by RTMo, and by including the fluorescence in the NO. The effect of fluorescence on the apparent reflectance (R_a) was modelled by including fluorescence radiance (F) in the simulated radiance (L):

$$\pi L = r_{so} E_{sun} + r_{do} E_{sky} + F \tag{2}$$

$$R_a = \frac{\pi L}{E_{sun} + E_{sky}}, \tag{3}$$

where r_{so} and r_{do} are the reflectance of solar and diffuse radiation, respectively, simulated by RTMo, and E_{sun} and E_{sky} are solar and sky irradiance spectra ($\mathrm{Wm}^{-2}\mu\mathrm{m}^{-1}$) estimated from a MODTRAN5 simulation for a clear sky atmosphere with solar zenith angle of 45°, air and vapour pressure and carbon dioxide and oxygen partial pressures of 967 hPa, 15 hPa, 364.4 ppm and 19.49 percent (note that the CO_2 concentration was somewhat low even for mid-growing season agricultural fields, but this does not affect the reflectance in the region of 400-900 nm). The direct and diffuse irradiance were calculated from MODTRAN5 output as:

$$E_{sun} = \pi t_1 t_4, \tag{4}$$

$$E_{sky} = \frac{\pi t_1 \left(t_5 + t_{12} r_{sd}\right)}{1 - t_3 r_{dd}}, \tag{5}$$

where t_i are atmospheric radiative transfer functions of MODTRAN5: t_1 is the extraterrestrial solar irradiance ($\mathrm{Wm^{-2}\mu m^{-1}sr^{-1}}$), t_3 the spherical albedo, t_4 the direct solar transmittance, t_5 the diffuse solar transmittance, and t_{12} the product of t_3 and t_4 (see Fig. 2 in Cogliati et al. (2015b)), all averaged to the resolution of the field spectrometer. The fluorescence spectra in Eq. (2) were not computed with the full SCOPE model, but instead simulated as a linear combination of four basis spectra, derived from output of earlier SCOPE runs using principal component (PC) analysis. Four coefficients, one for each of these basis spectra, were retrieved. The fluorescence spectra retrieved in this way, however, were only intended to correct for the spike in the apparent reflectance. The values at 760 nm were reasonably in agreement with the SFM data from the much higher spectral resolution measurements, but we consider the latter as measured fluorescence.

The following parameters were retrieved: Leaf Area Index LAI ($\mathrm{m^2\ m^{-2}}$), Leaf Inclination Distribution Function parameters $LIDFa$ and $LIDFb$, leaf chlorophyll a+b concentration C_{ab} and leaf carotenoid concentration C_{ca} (μg $\mathrm{cm^{-2}}$), leaf dry matter C_{dm} and leaf water C_w concentration (g $\mathrm{cm^{-2}}$), brown pigment C_s (arbitrary unit), and four coefficients C_{1-4} for the fluorescence PC's. The mesophyll scattering parameter N was fixed to 1.5. Parameters $LIDFa$ and $LIDFb$ are used to describe the cumulative probability distribution function of leaf inclination angles mathematically (Verhoef, 1998; Wang et al., 2007). $LIDFa$ determines the average leaf inclination (-1 for planophile (9°) and +1 for erectophile (89°) leaves), and $LIDFb$ the bimodality of the distribution.

2.4. Simulation of fluorescence

We simulated diurnal cycles of SIF with the retrieved parameter values using half-hourly synoptic data from an on-site weather station as input with the complete SCOPE model, while the leaf and canopy parameters were maintained constant during each day. Several model parameters that affect the emission efficiency of SIF but not R, such as carboxylation capacity at 25°C, V_{cmo}, and the Ball-Berry parameter for the calculation of the stomatal conductance, m

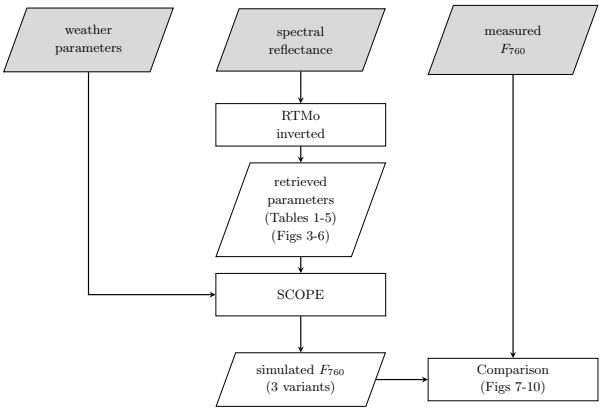

Figure 2: Schematic overview of the procedure to compare simulated fluorescence to observations

(Verrelst et al., 2015), were maintained at default values. It is common practice to treat these as constants during a diurnal cycle, but PQ and NPQ are still variable: They are functions of irradiance, temperature, relative humidity and wind speed. The MODTRAN irradiance spectra E_{sun} and E_{sky} were linearly scaled at every 30-minute time interval to match exactly the instantaneously measured broadband irradiance. To investigate the effect of variations in fluorescence emission efficiency under natural conditions relative to the effects of leaf composition, leaf area and leaf inclination, three types of simulations of SIF were carried out:

1. The reference simulation. A simulation in which the fluorescence emission efficiencies at photosystem level were kept constant over time. The emission efficiency calculated by the biochemical routine was overruled in an extra line added to the code in the model. For this constant emission efficiency, we used the default value of 0.002 for PSI, while for PSII we chose the (peak) value as simulated with the biochemical model of Van der Tol et al. (2014) at intermediate light conditions (the peak value in Fig. 1a.), and applied this value throughout the day. The total efficiency (of PSI and PSII) between 700 and 760 nm was 1.44 times the efficiency under low light, unstressed condition. In this way physiological regulation of photosynthesis and SIF was 'switched off'. This enabled us to quantify the effects of leaf composition, leaf area and leaf inclination on SIF and on the efficiency of SIF (i.e., SIF/irradiance) at canopy level. The SIF of this reference simulation is proportional to irradiance, and otherwise only a function of R, and is independent of, for example, the carboxylation capacity or the leaf temperature.
2. The dynamic simulation. A simulation in which the fluorescence efficiency was calculated with the standard SCOPE model, i.e., using the drought parameterization of Van der Tol et al. (2014). Wullschleger (1993) published tables of literature values of V_{cmo}: the average values therein were 94 μmol m^{-2} s^{-1} for rice and 67 μmol m^{-2} s^{-1} for all C3 crops together.

Here we used V_{cmo} = 80 μmol m^{-2} s^{-1}. The Ball-Berry parameter for stomatal regulation m was set to 10, such that stomatal conductance varied with relative humidity, and the simulated internal CO_2 concentration in the stomata was about 70 percent of the ambient at the mean midday relative humidity. The dynamic simulation yields lower values for SIF than the reference simulation.

3. A simulation with (constantly) inhibited PQ. In this simulation the maximum stress effect of a fully blocked photochemical pathway was calculated. From the values of the rate coefficients for kinetics in the model of Van der Tol et al. (2014), we can derive that the maximum possible effect of blocked PQ is a factor 5 increase in fluorescence of PSII compared to that of untreated vegetation under low light, and a factor 3.3 increase compared to the reference simulation as defined earlier. We therefore carried out a simulation in which we forced the fluorescence efficiency of photosystem II to be 5 times the default value for low light unstressed vegetation, thus overruling the value computed by the physiogical model in the code. This simulation was carried out only for the treated grass.

The differences between the simulations, and between measured and simulated SIF, provide insight into the magnitude of the effect of PQ and NPQ on SIF, as compared to the effects of leaf composition, leaf area and leaf inclination. The focus here is on the diurnal shape, while the absolute values of SIF have some uncertainty due to the chosen value of the emission efficiencies at low light. The results of the reference and dynamic simulation were both qualitatively compared to observations of chlorophyll fluorescence at 760 nm (F_{760}) and differences between days and times of the day were analysed.

2.5. Model sensitivity and error propagation

The Jacobian of the model was calculated to determine (i) the most influential parameters for reflectance and fluorescence of the crops and the grass, (ii) the ill-posedness of the retrieval, and (iii) the propagation of retrieval errors into the simulated fluorescence. Two Jacobians were computed for each set of

optimized parameters: J_R, which is the local model sensitivity of R at each λ_i of the b spectral bands of the HR4000 spectrometer to each of the $n = 12$ parameters, and J_F, which is the local model sensitivity of the SIF spectrum at each fluorescence wavelength (640-850 nm, 1 nm resolution) to each parameter:

$$J_R = \begin{bmatrix} \partial R_{\lambda 1}/\partial p_1 & \dots & \partial R_{\lambda 1}/\partial p_n \\ \vdots \dots & \ddots & \vdots \\ \partial R_{\lambda b}/\partial p_1 & \dots & \partial R_{\lambda b}/\partial p_n \end{bmatrix} \tag{6}$$

and

$$J_F = \begin{bmatrix} \partial F_{640}/\partial p_1 & \dots & \partial F_{640}/\partial p_n \\ \vdots \dots & \ddots & \vdots \\ \partial F_{850}/\partial p_1 & \dots & \partial F_{850}/\partial p_n \end{bmatrix} \tag{7}$$

The Jacobians were further normalized (multiplied) by the span of each parameter to obtain comparable numbers in equal units, and then analysed by decomposing them into singular values and singular vectors using Singular Value Decomposition (SVD):

$$J_N = U \Sigma V^\top, \tag{8}$$

where the subscript N stands for normalized Jacobian, U and V are the left and right singular vectors, respectively, and Σ is a diagonal matrix of singular values. U is a matrix of 12 spectra (in columns), and V is a 12x12 matrix providing the contributions of each of the 12 parameters in Table 1 to each spectrum in U. The occurrence of relatively low singular values indicates ill-posedness.

We estimated the propagation of uncertainty in the measured reflectance spectra into the model simulations of fluorescence by first calculating the uncertainty (i.e., the standard deviation) in model parameters, σ_p:

$$\sigma_p = (J_R^\top J_R)^{-1} J_R^\top \sigma_R^\top \tag{9}$$

where σ_R the spectrum of uncertainty in R. The covariance matrix of simulated SIF, c_{SIF}^2 is:

$$c_{SIF}^2 = J_F(\sigma_p \sigma_p^\top) J_F^\top, \tag{10}$$

and the variance is the diagonal of the covariance matrix, which is a spectrum from 650 to 850 nm. From this matrix, we selected only the value at index (i, i) for which $wl = 760$ nm, and calculated the standard deviation of F_{760} as the square root of this value:

$$\sigma_{F760} = \sqrt{c^2_{SIF}(i, i)}. \tag{11}$$

For σ_R we used the standard deviation of repeated measurements of R of the same target on the same day, within two hours around solar noon. This provides a measure for the uncertainty due to variability in irradiance and instrumental noise, but it does not represent the total measurement uncertainty, which would also include instrument calibration errors. This methodology provides the minimum uncertainty in simulated SIF that can be expected.

3. Results

3.1. Parameter retrievals from reflectance spectra

Figs. 3 and 4 show the simulated reflectance on 7 and 4 dates during the growing season of rice and alfalfa, respectively, along with the measured apparent reflectance, and Fig. 5 shows the reflectance of the control and treated grass on two days. Alfalfa was cut on Julian day of the year 180 (DOY=180), and the first spectrum corresponds to the mid-season phase, whereas the other three spectra show the crop development phase after regrowth. In general, the model reproduces the reflectance well (RMSE between 0.0032 and 0.0106). The four reflectance spectra of the grass are similar: there are only small differences between the two dates and between the two plots. The residuals (the measured minus simulated spectra) are shown as well, and these are in the same order of magnitude as, but somewhat higher than, the standard deviation of the measurements for most wavelengths. The following discrepancies between simulated and measured spectra are evident. It appears that in some cases the simulated reflectance peak in the green (550 nm) is too sharp (for example DOY 248 for rice). We attribute this to the absorption spectra of carotenoids and chlorophyll

used as input of Fluspect. Spikes in the NIR can be attributed to atmospheric effects: The spectra of direct and diffuse incident light were not measured separately, and here MODTRAN simulated spectra have been used. Spikes at 720 and 880 nm can be attributed to effects of water vapour absorption, and the spike at 760 nm to either an inaccuracy in the O_2-A absorption band depth, or a mismatch in the shape of the simulated ChlF. ~~At the red edge the residuals are larger, which could be explained by the fixed absorption spectra of the leaf constituents. With the PCs for the fluorescence, the spike in reflectance at 760 nm could only partly be reproduced and some discrepancy remains. This may be caused by the fact that the spectral distibution of the fraction diffuse:direct irradiance, which affects the spike, was not known exactly. The relatively large differences between measured and simulated spectra around 890 nm in alfalfa may have the same cause: In this region the diffuse and direct light, which have a different reflectance due to directionality, are strongly different spectrally.~~

Fig. 6 and Table 2 show a representative example of the results of the SVD of normalized J_R, for alfalfa on DOY=164. The nearly four orders of magnitude difference between the highest and lowest singular value (SV) indicates that the retrieval was ill-posed. The four fluorescence coefficients dominate the lower SV values. This is expected: Their contribution is concentrated in a few bands only (Fig 6), and therefore these SVs are small. The largest SV is dominated by C_{dm} and LAI, but with an opposite sign, which indicates that the effects of parameters can to some degree nullify, such that an overestimate (underestimate) in one can be accompanied by an overestimate (underestimate) in the other. The second SV is dominatd by C_{ab}, and the third by C_s. The fourth to eighth SVs are $< 5\%$ of the first; these are dominated by C_{ca}, C_w and combinations of other parameters. Although the leaf inclination distribution parameters only dominate small SV, they also have some effect on the first three highest SVs.

The retrieved parameter values are listed in Tables 3 to 5. The retrieved C_{ab} and C_{dm} decreased over time in rice, while C_s increased. These are realistic patterns, but a few other features are not. On one day in both in rice and alfalfa, retrieved C_{dm} was zero. Due to the ill-posedness of the inversion, these

values were compensated by LAI values lower than expected.

Table 2: Singular values (SV) and right singular vectors (V) of the Jacobian of the reflectance model after fitting to the measured reflectance of alfalfa on DOY=164. The highest contributions per SV is shown in bold font. The squared sum over rows equals 1, and likewise the squared sum over columns equals 1.

SV	12.4	4.08	1.3217	0.597	0.281	0.200	0.106	0.081	0.059	0.032	0.006	0.004
rank	1	2	3	4	5	6	7	8	9	10	11	12
C_{ab}	0.09	**0.94**	0.18	-0.08	-0.25	0.06	0.01	0.00	0.00	0.01	0.00	-0.00
C_{dm}	**0.75**	-0.16	0.12	-0.10	-0.16	0.38	-0.44	0.12	-0.07	0.01	-0.02	-0.02
C_w	0.06	-0.03	0.15	-0.02	0.21	**0.68**	**0.65**	-0.06	-0.06	-0.18	0.01	-0.00
C_s	0.24	0.16	**-0.94**	0.05	0.02	0.05	0.13	0.01	-0.04	-0.02	-0.01	0.00
C_{ca}	0.00	0.04	0.05	**0.98**	-0.13	0.12	-0.06	0.04	0.01	-0.01	-0.00	0.00
LAI	-0.48	0.15	-0.13	-0.04	0.39	0.47	-0.56	0.14	-0.16	-0.03	-0.03	-0.03
$LIDFa + LIDFb$	-0.26	-0.13	-0.11	-0.09	-0.58	0.23	-0.01	0.03	-0.04	0.03	**0.70**	0.02
$LIDFa - LIDFb$	-0.27	-0.14	-0.09	-0.10	**-0.59**	0.21	0.02	0.06	0.08	-0.02	**-0.70**	-0.02
$C1$	-0.00	-0.02	0.03	0.03	-0.08	-0.09	0.06	-0.22	**-0.95**	0.15	-0.08	-0.06
$C2$	-0.00	0.00	0.04	-0.01	0.02	-0.11	0.19	**0.95**	-0.19	0.06	0.01	0.02
$C3$	-0.00	-0.00	-0.01	0.00	0.07	0.16	0.08	-0.04	0.15	**0.96**	-0.03	0.08
$C4$	-0.00	0.00	0.00	-0.00	-0.00	0.01	-0.03	-0.02	-0.07	-0.07	-0.03	**0.99**

3.2. Solar induced fluorescence simulations

With the retrieved parameter values, the diurnal cycles of SIF were simulated. Table 6 shows the SVD of the normalized Jacobian of SCOPE fluorescence spectra J_F for alfalfa on DOY=164. Again, C_{dm} dominates the first SV, but all other parameters except for C_w and C_{ab} also contribute to the highest SV. The second SV is dominated by C_{ab}, which has a specific effect on the shape of the fluorescence spectrum: The higher C_{ab}, the higher the ratio of near infrared to red fluorescence; this specific effect causes C_{ab} t~~d~~o dominate one specific SV. The third SV is dominated by leaf inclination distribution $LIDFa$, C_{dm}, C_s and C_{ab}. Only the fifth SV is dominated by LAI, but the fourth to the eighth SVs are all rather small ($< 5\%$ of the first SV). Similar to reflectance, the effects of C_{dm} and LAI have opposite signs in the first two SVs. We discussed earlier that these parameters are likely to be simultaneously overestimated or underestimated. The fact that the effects of C_{dm} and LAI on fluorescence are also opposite implies that the effect of a simultaneous overestimate or underestimate

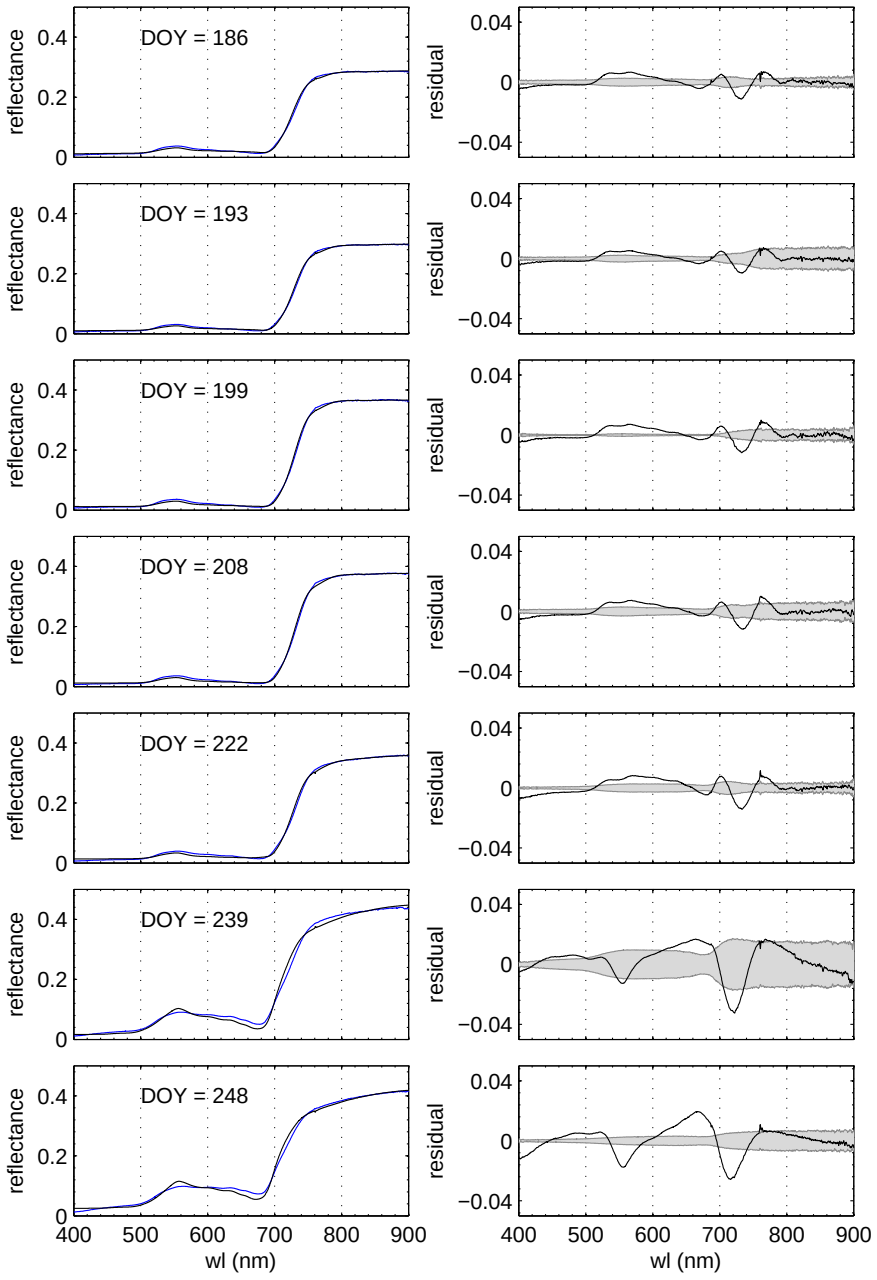

Figure 3: Left panels: Measured (blue) and simulated (black) midday apparent reflectance spectra on seven Julian days for a rice growing season. Right panels: the residual after spectral fitting (i.e., the difference between measured and simulated apparent reflectance (line)), and the standard deviation of the measurements (gray shaded area).

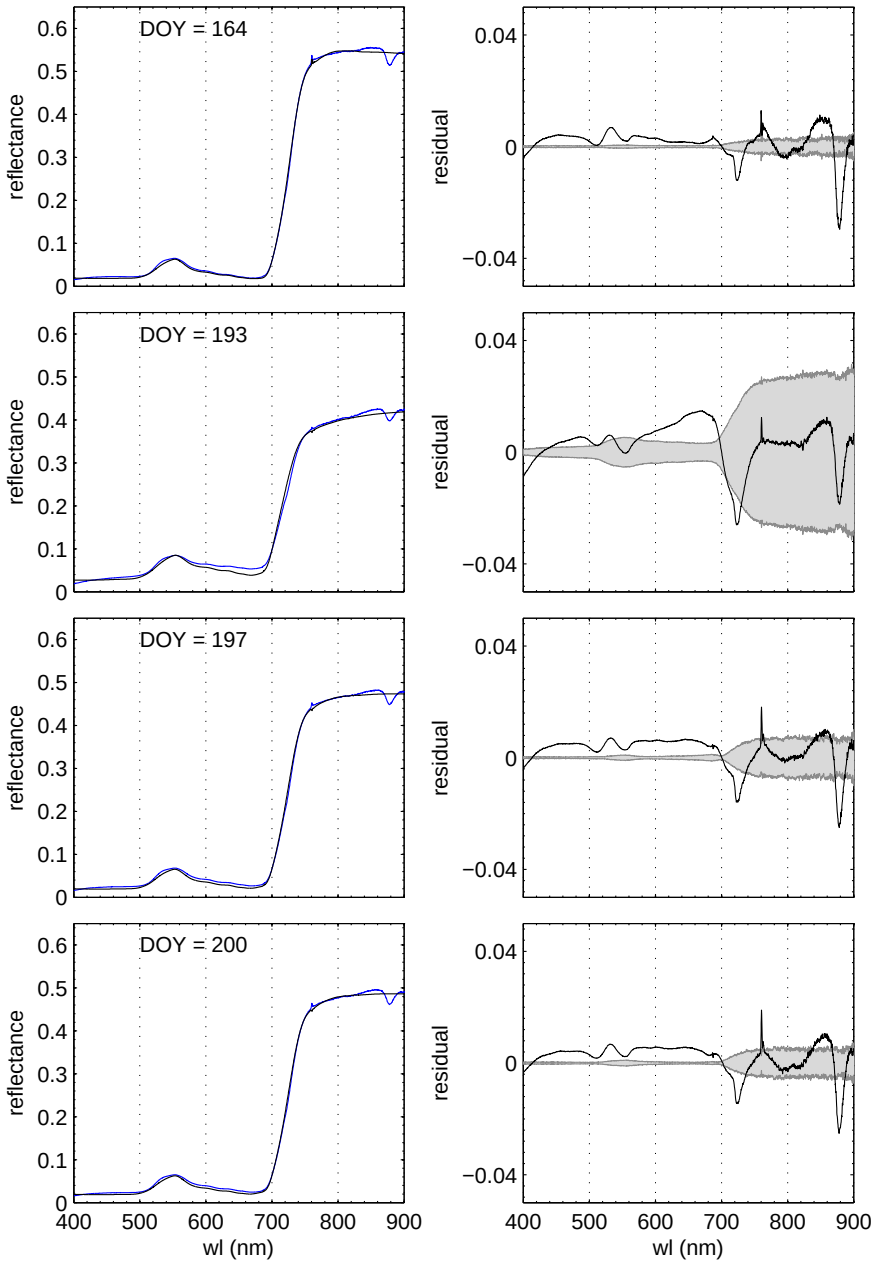

Figure 4: Left panels: Measured (blue) and simulated (black) midday apparent reflectance spectra on four selected Julian days for alfalfa. The crop was mowed on DOY=180. Right panels: the residual after spectral fitting (i.e., the difference between measured and simulated apparent reflectance (line)), and the standard deviation of the measurements (gray shaded area).

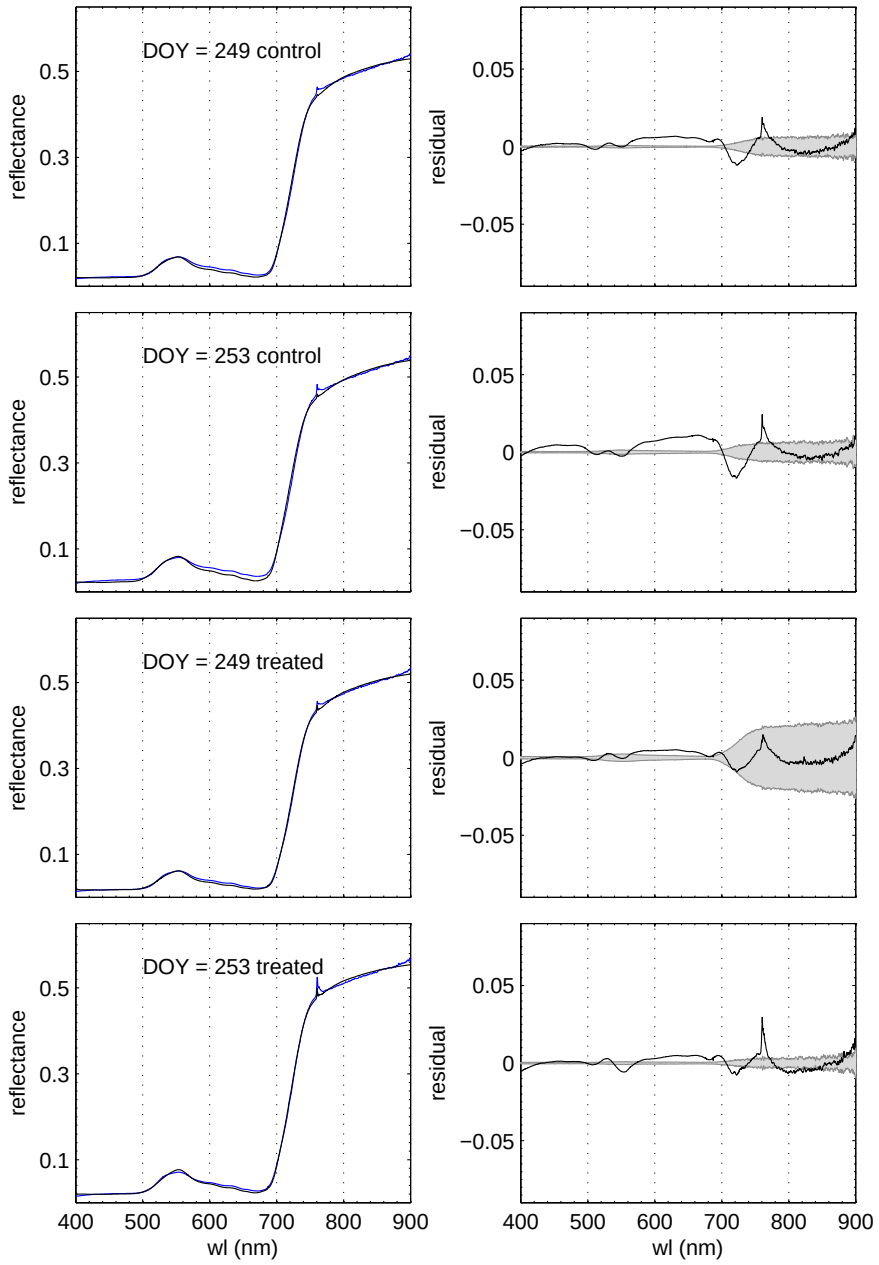

Figure 5: Measured and simulated midday apparent reflectance spectra of a control and a DCMU treated grass for two days. Right panels: the residual after spectral fitting (i.e., the difference between measured and simulated apparent reflectance (line)), and the standard deviation of the measurements (gray shaded area).

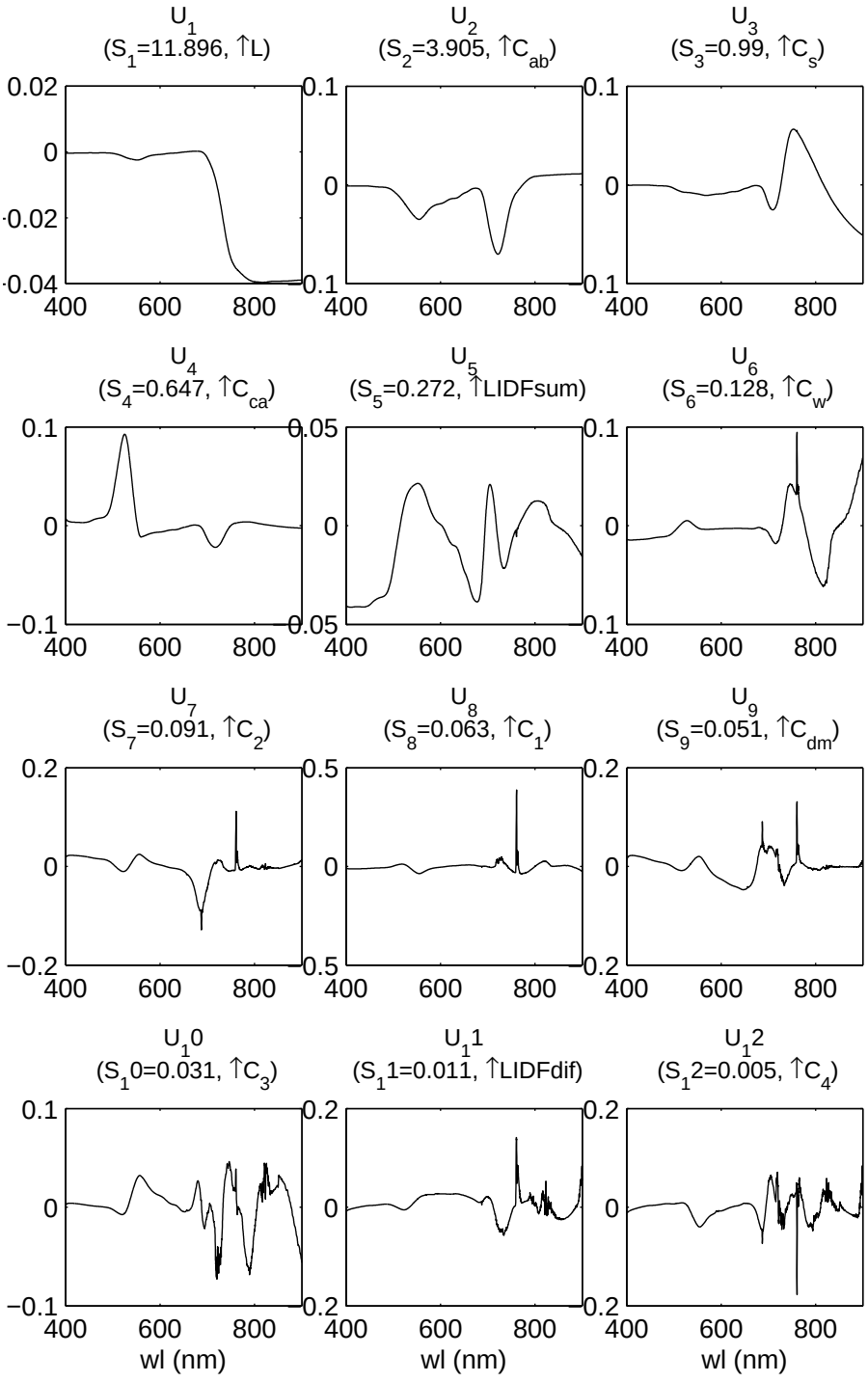

Figure 6: Left singular vectors U of the Jacobian of the reflectance model for alfalfa DOY=164. The weights S of the vectors and the most contributing parameter are provided in the caption of each subplot. Refer to Table 2 for the SV and rank of each of the 12 parameters in Table 1.

Table 3: Parameter values for rice as retrieved from mid-day hyperspectral reflectance measurements for seven days in the growing season of rice with the RTMo model of SCOPE.

DOY	186	193	199	208	222	239	248
C_{ab} (μg cm^{-2})	55	60	61	60	57	12	13
C_{dm} (mg cm^{-2})	5.0	4.7	4.2	3.3	2.9	2.0	0.0
C_s (a.u.)	0.07	0.07	0.04	0.06	0.15	0.26	0.39
C_w (mg cm^{-2})	21	21	21	20	19	24	16
C_{ca} (μg cm^{-2})	9.5	9.7	9.4	9.5	9.5	5.2	7.3
LAI (m^{2}m^{-2})	2.8	3.3	3.5	3.6	2.9	3.8	1.6
$LIDFa$	-0.79	-0.82	-0.64	-0.65	-0.60	-0.41	0.22
$LIDFb$	-0.15	-0.15	-0.15	-0.15	-0.15	-0.11	-0.12
$RMSE$ of refl	0.0036	0.0032	0.0040	0.0042	0.0049	0.0106	0.0092

of retrieved C_{dm} and LAI cancels out in the simulation of fluorescence. Thus one can to some degree predict fluorescence from reflectance correctly for the wrong reasons (i.e., parameters), as long as the measured reflectance spectrum is reproduced.

The diurnal cycles of SIF at 760 nm (F_{760}), normalized by the incident photosynthetically active radiation (PAR) in energy units (Wm^{-2}) are shown in Figs 7 and 8. The resulting normalized SIF can be considered as an efficiency, but it only represents the emission at one wavelength (760 nm), and only in one solid angle, therefore it is expressed in μm^{-1} sr^{-1}. The normalization by irradiance i.e., the computation of apparent fluorescence yield is necessary because otherwise variations in SIF are dominated by the diurnal cycles of irradiance, and this makes it more difficult to visualize and comprehend the effects of pigments, leaf area and leaf inclination, and physiology. Figs. 7 and 8 show how these simulations compare to observations (irradiance is shown separately). We plotted the half-hourly observations along with the reference simulations (dashed lines) and the dynamic simulations (solid lines). Shown as grayscale around the reference simulation is the uncertainty of the reflectance measurements propagated into F_{760} ($F_{760} + / - \sigma_{F760}$) as calculated with Eq. (11).

Table 4: Parameter values as retrieved from mid-day hyperspectral reflectance measurements for four days in the growing season of alfalfa with the RTMo model of SCOPE.

DOY	164	193	197	200
C_{ab} (μg cm^{-2})	42	33	40	41
C_{dm} (mg cm^{-2})	2.8	0.0	3.4	3.4
C_s (a.u.)	0.00	0.18	0.05	0.04
C_w (mg cm^{-2})	23	15	21	20
C_{ca} (μg cm^{-2})	8.0	6.7	7.2	7.7
LAI (m^{2}m^{-2})	4.2	1.4	3.0	3.3
$LIDFa$	-0.04	0.45	0.01	-0.02
$LIDFb$	-0.15	-0.13	-0.13	-0.13
RMSE of refl	0.0055	0.0085	0.0060	0.0056

There are differences between clear-sky days in measured normalized F_{760} for both rice and alfalfa. These differences are reproduced by both the reference and the dynamic simulation (in all subplots in Figs 7 and 8, representing the days, the simulations are close to the measurements). The fact that the reference simulation (with a constant fluorescence emission efficiency) also reproduces the differences between days, implies that we can explain a large part of the seasonal cycle of normalized F_{760} from the parameters that were retrieved from R on clear sky days. In other words, the information contained in F_{760} overlaps with the information contained in the reflectance of these healthy, well developed crops. To illustrate this more clearly, we have also plotted the daily averages of normalized F_{760} versus Julian day for the rice crop in Fig. 9. The seasonal pattern of simulated fluorescence is similar to the measured pattern. Most of the measurements fall between the reference simulation and the dynamic simulation.

There is no clear diurnal signal in the measured normalized F_{760} (Figs. 7 and 8). The measured normalized F_{760} of rice tends to decline towards the afternoon for most days, whereas the measured normalized F_{760} in alfalfa tends to increase towards the afternoon. These variations are nevertheless small, indicating that F_{760} is almost proportional to irradiance during each day. The

Table 5: Parameter values as retrieved from mid-day hyperspectral reflectance measurements for two days of control and DCMU treated grass with the RTMo model of SCOPE.

DOY	249 control	249 treated	253 control	253 treated
C_{ab} (μg cm^{-2})	33	27	35	30
C_{dm} (mg cm^{-2})	2.5	2.8	2.2	2.1
C_s (a.u.)	0.20	0.21	0.19	0.15
C_w (mg cm^{-2})	13.6	14.4	13.1	10.3
C_{ca} (μg cm^{-2})	7.4	5.8	8.4	7.8
LAI (m^{2}m^{-2})	4.1	4.1	4.1	4.3
$LIDFa$	-0.03	0.06	-0.16	-0.02
$LIDFb$	-0.13	-0.13	-0.13	-0.13
RMSE of refl	0.0050	0.0067	0.0041	0.0047

reference simulation also has a weak diurnal cycle, caused by the diurnal cycle of the solar zenith angle. The solar zenith angle affects the distribution of light over leaves: a more horizontal solar beam penetrates less deeply into the canopy than a more vertical solar beam, and this in turn affects the emission of fluorescence. As expected, the dynamic simulation which also accounts for the effects of weather conditions on PQ and NPQ, produced lower normalized F_{760}, and a slightly different diurnal cycle. The difference between the two simulations is small compared to the actual values of normalized F_{760}. Although the dynamic simulation is somewhat closer to the measurements than the reference scenario, it does not necessarily reproduce the diurnal variations better than the reference simulation. In the rice crop, the measurements are closer to the reference scenario in the morning hours, and drop to the physiologically regulated level in the afternoon, while the opposite is the case for alfalfa. The diurnal cycle potentially contains some information about the physiological regulation of the signal, but the scatter in the data is too large to draw firm conclusions.

Because we did not have experimental data of a naturally stressed crop, we induced the effects of changing PQ by chemically reducing and blocking the electron transport by means of the herbicide DCMU to provoke a functional

Table 6: Singular values (SV) and right singular vectors (V) of the Jacobian of fluorescence spectra simulated with SCOPE after fitting to the measured reflectance of alfalfa on DOY=164. The highest contribution(s) in each column is indicated by bold font.

SV	12.1	6.0	1.46	0.61	0.21	0.095	0.014	0.006
rank	1	2	3	4	5	6	7	8
C_{ab}	-0.01	**0.87**	0.39	0.27	0.04	0.10	0.01	0.01
C_{dm}	**-0.57**	-0.22	0.37	0.05	**0.70**	0.03	0.02	-0.01
C_w	-0.03	-0.02	0.00	0.03	-0.01	0.19	**-0.97**	0.12
C_s	-0.45	-0.06	0.40	-0.45	-0.58	0.31	0.07	0.02
C_{ca}	-0.45	0.15	-0.12	0.02	-0.22	**-0.83**	-0.13	0.10
LAI	0.29	0.23	0.10	**-0.83**	0.33	-0.23	-0.09	-0.01
$LIDFa + LIDFb$	0.26	-0.22	0.51	0.14	-0.13	-0.28	-0.14	**-0.70**
$LIDFa - LIFDb$	0.34	-0.26	**0.52**	0.13	-0.06	-0.21	0.05	**0.70**

change. Blocking the photochemical dissipation pathway would cause a lower total (PQ+NPQ) quenching rate of the excitation, resulting in a higher F_{760} than in untreated vegetation. Indeed we observed that measured F_{760} of the control plot followed the dynamic simulation on 5 September, while F_{760} of the treated lawn quickly rose to values above controls but below those of the dynamic simulation after reducing PQ in the morning by a small dose of DCMU. The fluorescence remained above controls but below the dynamic simulation throughout the day (Fig. 10). Because of the lower dose of DCMU, electron transport at PSII might not have been completely blocked, and some NPQ still may have been in operation, which could have accounted for the F_{760} value of the treated grass being substantially lower than its simulated theoretical maximum. On 9 September, the electron transport was fully blocked by applying a tenfold higher concentration of DCMU. In that case F_{760} of the treated lawn approached the simulation of the theoretical maximum for PQ=0 and NPQ=0, while F_{760} of the control lawn was still close to the dynamic simulation.

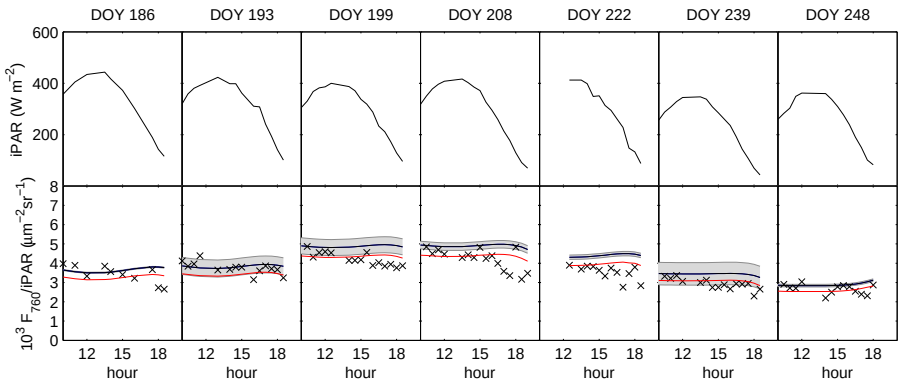

Figure 7: Measured PAR irradiance (top) and diurnal cycles of simulated (lines) and measured (symbols) F_{760} normalized by incident PAR for selected dates in the rice's growing season ~~of rice~~ (bottom). The black solid line represents a model simulation with maximum ChlF emission efficiency and the shaded area two times the standard deviation calculated with Eq. (11), whereas the ~~blue~~red solid line represents a simulation in which fluorescence emission efficiency was calculated from weather conditions and parameters carboxylation capacity V_{cmo} and Ball-Berry stomatal parameter m.

4. Discussion

In this study, we have presented a methodology to retrieve parameters from field hyperspectral R, and to further use these parameters to simulate ~~energy fluxes, reflectance, photosynthesis and~~ SIF. The simulated normalized F_{760} reproduced most of the temporal variability retrieved from high resolution spectra collected in the field. The diurnal variability of normalized F_{760} was low in both rice and alfalfa. This is empirical evidence for the finding of Verrelst et al. (2015) that parameters of physiological regulation (V_{cmo} and m) and weather variables have a relatively small effect on normalized F_{760}. Verrelst et al. (2015) also found that the effect of the parameters C_{ab} and C_s declined with fluorescence wavelength. We found that these two parameters still have a considerable effect on the fluorescence variability at 760 nm, besides C_{dm}, LAI and the leaf inclination distribution. Several other factors contributed to the limited signal in the diurnal cycle of normalized F_{760}. First, accurate early morning and late

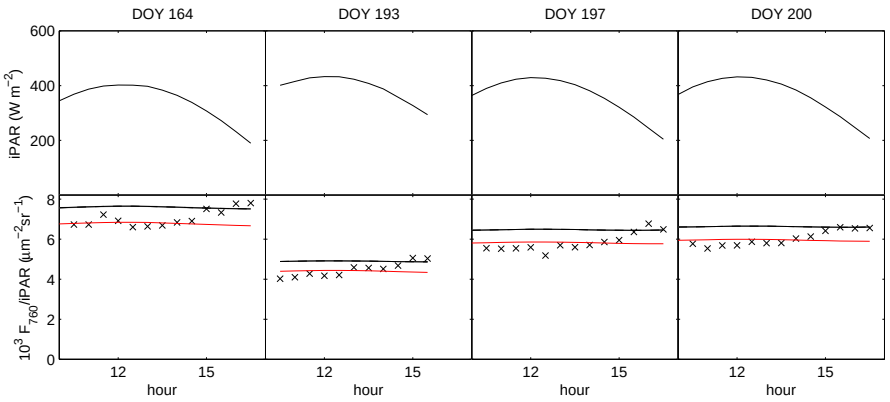

Figure 8: Measured PAR irradiance (top) and diurnal cycles of simulated (lines) and measured (symbols) F_{760} normalized by incident PAR for selected dates in the growing season of alfalfa (bottom). The black solid line represents a model simulation with maximum fluorescence emission efficiency, whereas the red line represents a simulation in which fluorescence emission efficiency was calculated from weather conditions and parameters V_{cmo} and m. Note that the crop was mowed on DOY=180. Around the black line, a shaded area is plotted indicating two times the standard deviation calculated with Eq. (11), but this is barely visible because the standard deviation was small.

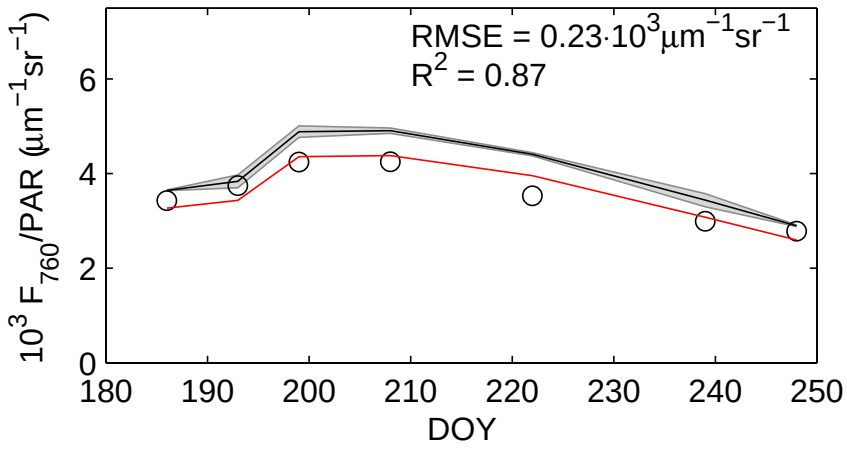

Figure 9: Diurnal cycles of simulated (lines) and measured (symbols) daily average F_{760} normalized by daily average PAR for selected dates in the growing season of rice. The black solid line represents a model simulation with maximum fluorescence emission efficiency and the shaded area two times the standard deviation calculated with Eq. (11), whereas the ~~blue~~red line represents a simulation in which fluorescence emission efficiency was calculated from weather conditions and parameters V_{cmo} and m, but for daily averages of the normalized F_{760}. The $RMSE$ and R^2 are presented for the dynamic simulation and the measurements.

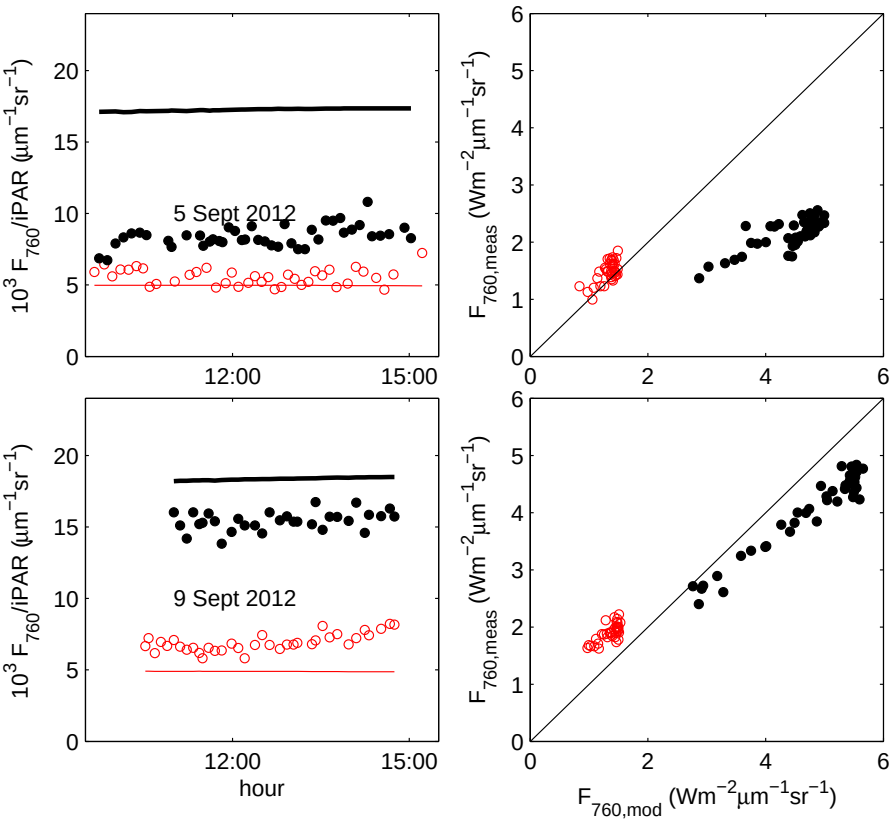

Figure 10: Left: Measured (symbols) and modelled (lines) diurnal cycles of irradiance normalized F_{760} of two grass plots: a control (open symbols/ fine line), and a treated plot in which PQ was (partially) blocked (filled symbols/ bold line). The fine (red) line denotes the dynamic simulation and the bold line the simulation with maximum DCMU effect. On 5 September (top), PQ was only partially blocked after application of DCMU in solution with a concentration of 10^{-5}M in 1% ethanol/water, whereas on 9 September (bottom), PQ was fully blocked after application of DCMU in solution with a concentration of 10^{-4}M in 1% ethanol/water. The simulation of the treated plot assumed the maximum possible effect of DCMU. Right: the same data plotted as modelled versus measured F_{760}. Here F_{760} was not normalized to enhance legibility and better separate the points in the graph. The solid line is the 1:1 line.

afternoon measurements were not available. Measurements around midday are reliable, but as the solar zenith angle increases, it becomes increasingly difficult to retrieve F_{760} with high confidence. The retrieval relies on accurate measurements of the incident light as well as representative measurements of the canopy. Both are problematic in the first hours after sunrise and the hours before sunset. For this reason the seasonal cycle analysis was limited to approximately 10AM to 4PM, which limits the time span of the diurnal cycle. Second, the rice and alfalfa crops studied here were agricultural crops, supplied with sufficient water and nutrients throughout the season. In the absence of any stress, it is likely that the fluorescence emission efficiency was not highly variable. Lower fluorescence efficiency and higher NPQ during heat or drought (Ač et al., 2015) or light saturation (Van der Tol et al., 2014) and higher fluorescence during chilling especially of non-cold-hardy plants (Ač et al., 2015; Lindfors et al., 2015) can be expected. For example, Zarco-Tejada et al. (2013) found not only significant correlations between gross primary productivity (GPP) and spectral indices for chlorophyll content, but also between GPP and chlorophyll fluorescence and photochemical reflectance index over a seasonal cycle in an olive orchard. At the same time, vegetation indices for vegetation structure did not correlate with GPP. In that case, physiological changes affecting the fluorescence emission efficiency could have been responsible for the observed correlation, but in our study, stress conditions did not occur in the rice and alfalfa crop. The experiment in which the electron transport of PSII was inhibited in grass clearly demonstrated that F_{760} can be used to reveal variations in PQ. Combining the reference scenario with the scenario of complete blocking of electron transport enabled us to estimate the maximum effect of this type of artificially induced environmental stress, and the dynamic changes in F_{760} were in agreement with our expectation and with modelling results.

Two model limitations need to be considered. We have already indicated that the absolute levels of simulated F_{760} were not certain. In addition, the model of Van der Tol et al. (2014) that was used to simulate leaf-level variations in PQ and NPQ is parameterized using empirical data, and may not apply to all

conditions in the field. Even in Van der Tol et al. (2014) two empirical fits were presented: one for several species in outdoor conditions under natural drought, and one for cotton in laboratory conditions. The difference in diurnal shape between the alfalfa and rice crops could be due to a different response of NPQ to irradiance. Diurnal cycle measurements in combination with modelling as described in this paper, could be used to further study the effects of NPQ of F_{760} in different crops if sufficient data are available.

Our finding of a limited effect of physiological regulation on F_{760} seems to contradict a recent study, in which SCOPE has been used to retrieve the photosynthetic capacity parameter V_{cmo} from changes in emission efficiency as observed by the GOME-2 satellite product of SIF for coarse spatial scales (e.g., 0.5°) in regions that include ~~over~~ large agricultural fields in the USA (Zhang et al., 2014). ~~A comparison between the studies is, however, hardly possible. Although~~ The SCOPE model was used in both instances, but the two studies are very different in temporal and spatial scale. Here, we have focussed on a small number of diurnal cycles, but Zhang et al. (2014) used satellite data acquired in the early morning (9:30am) as compared with our midday field measurements, and those data were aggregated over space and time over the entire growing season. Our local-scale ground-based results suggest that the effect of leaf pigments, leaf area and leaf inclination is much stronger than the effect of the emission efficiency on fluorescence. It is possible that during entire growing seasons including drought and senescence, the effects of PQ and NPQ (and thus V_{cmo}) become more apparent. An alternative explanation for the apparent contradiction between Zhang et al. (2014)'s and the present findings, is that we were able to estimate the scattering and (re-)absorption from the whole reflectance spectrum as compared to only a few satellite bands. This enabled us to better 'correct' for the effects of leaf pigments and canopy structure on the absorbed photosynthetically active radiation (aPAR), and thus the light use efficiency. Without the quantification, variations SIF caused by pigment content and vegetation structure may be attributed to effects of PQ and NPQ, and thus to V_{cmo}. It is still an open question which spectral information is

essential, and whether a method can be developed to obtain PQ and NPQ from satellite products from SIF in a more simple way than that presented here.

~~Furthermore, the retrieved V_{cmo} values may still 'contain' other effects. V_{cmo} is then not a strict leaf-level parameter but it compensates for effects of leaf pigments, leaf area and inclination that could not be retrieved from the MODIS products used by Zhang et al., (2014)~~

5. Conclusion

~~The SCOPE model was successfully used to reproduce the temporal variability of F_{760} in two unstressed crops. Most of the input parameters of the SCOPE model were retrieved from reflectance spectra measured in the field.~~

~~We conclude that~~ For a correct interpretation of variations in solar-induced fluorescence in terms of stress effects on PQ and NPQ, it is necessary to consider the variations in hyperspectral reflectance data. This study demonstrated that the SCOPE model is able to explain field measurements of F_{760} computed for three vegetation types and in different conditions, after parameter retrieval from hyperspectral data. Better results can be expected if the direct and diffuse irradiance spectra are measured separately in the field.

~~A s~~Sensitivity analysis performed on the SCOPE model for these crops showed that F_{760} values were mostly determined by C_{dm}, LAI, $LIDFa$, $LIDFb$, C_s and C_{ab}, which represent the canopy dry matter content, leaf area index, leaf inclination angles, brown pigment content and chlorophyll content. ~~This confirms the findings of Verrelst et al., (2015), who analysed the global sensitivity (i.e., the whole parameter space) of the model. The sensitivity analysis also showed that~~ The retrieval of parameter values from reflectance was ill-posed for C_{dm} and LAI. Both a high LAI and a low C_{dm} cause high scattering, and the cause of this scattering (LAI or C_{dm}) cannot be identified from the reflectance spectrum. The scattering appears to have ~~with~~ a similar effect on F_{760} and R.

In the crops, the diurnal variability of F_{760} normalized by the incident irra-

646 diance was low, probably because the physiological regulation of F_{760} emission
647 (through regulation of PQ and NPQ) during the day is low in healthy and un-
648 stressed canopy. ~~Simulations of F_{760} for a grass lawn with the electron transport~~
649 ~~of PSII blocked by a chemical agent showed that~~ In severely stressed conditions,
650 the effect of PQ and NPQ on fluorescence can nevertheless be estimated after
651 retrieval of C_{dm}, LAI, $LIDFa$, $LIDFb$, C_s and C_{ab}. This shows the impor-
652 tance of pairing F_{760} retrievals from specialized atmospheric chemistry satellites
653 (e.g., OCO-2) with VNIR spectrometer observations to acquire the necessary
654 canopy parameters that enable the interpretation of the SIF signal. Further
655 studies are necessary to validate models for the response of PQ and NPQ to
656 environmental conditions in naturally stressed vegetation. This can be achieved
657 with concurrent R and SIF measurements in vegetation exposed to a variety
658 of stresses.

659 ~~This~~ The proposed methodology is useful for future research. The study
660 also may help in defining a strategy using future FLEX data. In this con-
661 text, measurements of reflectance from the FLuORescence Imaging Spectrom-
662 eter (FLORIS) can be used in a inversion process to estimate biochemical and
663 biophysical parameters directly from FLEX, that can then be successfully used
664 to properly interpret the SIF signal.

665 **Acknowledgment**

666 Funding for this work was provided by the European Space Agency (ESA),
667 'FLEX/Bridge Study' (ESA/ESTEC Contract No. 4000112341/14/NL/FF/gp).
668 The first author received a travel grant to visit the Forschungszentrum Jülich in
669 the frame of the Transregional Collaborative Research Center (TR32) 'Patterns
670 in Soil-Vegetation-Atmosphere Systems: Monitoring, Modelling and Data As-
671 similation' funded by the Deutsche Forschungsgemeinschaft (DFG), which made
672 this work possible. We thank three anonymous reviewers for valuable comments
673 on the paper.

References

Ač, A., Malenovský, Z., Olejníčková, J., Gallé, A., Rascher, U., Mohammed, G., 2015. Meta-analysis assessing potential of steady-state chlorophyll fluorescence for remote sensing detection of plant water, temperature and nitrogen stress. Remote Sensing of Environment 168, 420–436.

Baker, N. R., 2008. Chlorophyll fluorescence: a probe of photosynthesis in vivo. Annual Review of Plant Biology 59, 89–113.

Cogliati, S., Rossini, M., Julitta, T., Meroni, M., Schickling, A., Burkart, A., Pinto, F., Rascher, U., Colombo, R., 2015a. Continuous and long-term measurements of reflectance and sun-induced chlorophyll fluorescence by using novel automated field spectroscopy systems. Remote Sensing of Environment 164, 270–281.

Cogliati, S., Verhoef, W., Kraft, S., Sabater, N., Alonso, L., Vicent, J., Moreno, J., Drusch, M., Colombo, R., 2015b. Retrieval of sun-induced fluorescence using advanced spectral fitting methods. Remote Sensing of Environment 169, 344–357.

Coops, N. C., Hilker, T., Hall, F. G., Nichol, C. J., Drolet, G. G., 2010. Estimation of light-use efficiency of terrestrial ecosystems from space: a status report. BioScience 60 (10), 788–797.

Damm, A., Elbers, J., Erler, A., Gioli, B., Hamdi, K., Hutjes, R., Kosvancova, M., Meroni, M., Miglietta, F., Moersch, A., et al., 2010. Remote sensing of sun-induced fluorescence to improve modeling of diurnal courses of gross primary production (GPP). Global Change Biology 16 (1), 171–186.

Damm, A., Guanter, L., Laurent, V., Schaepman, M., Schickling, A., Rascher, U., 2014. FLD-based retrieval of sun-induced chlorophyll fluorescence from medium spectral resolution airborne spectroscopy data. Remote Sensing of Environment 147, 256–266.

Drolet, G., Middleton, E., Huemmrich, K., Hall, F., Amiro, B., Barr, A., Black, T., McCaughey, J., Margolis, H., 2008. Regional mapping of gross light-use efficiency using modis spectral indices. Remote Sensing of Environment 112 (6), 3064–3078.

Franck, F., Juneau, P., Popovic, R., 2002. Resolution of the photosystem I and photosystem II contributions to chlorophyll fluorescence of intact leaves at room temperature. Biochimica et Biophysica Acta (BBA)-Bioenergetics 1556 (2), 239–246.

Frankenberg, C., Fisher, J. B., Worden, J., Badgley, G., Saatchi, S. S., Lee, J.-E., Toon, G. C., Butz, A., Jung, M., Kuze, A., et al., 2011. New global observations of the terrestrial carbon cycle from GOSAT: Patterns of plant fluorescence with gross primary productivity. Geophysical Research Letters 38 (17).

Frankenberg, C., O'Dell, C., Berry, J., Guanter, L., Joiner, J., Köhler, P., Pollock, R., Taylor, T. E., 2014. Prospects for chlorophyll fluorescence remote sensing from the Orbiting Carbon Observatory-2. Remote Sensing of Environment 147, 1–12.

Garbulsky, M. F., Peñuelas, J., Gamon, J., Inoue, Y., Filella, I., 2011. The photochemical reflectance index (PRI) and the remote sensing of leaf, canopy and ecosystem radiation use efficiencies: a review and meta-analysis. Remote Sensing of Environment 115 (2), 281–297.

Guanter, L., Frankenberg, C., Dudhia, A., Lewis, P. E., Gómez-Dans, J., Kuze, A., Suto, H., Grainger, R. G., 2012. Retrieval and global assessment of terrestrial chlorophyll fluorescence from GOSAT space measurements. Remote Sensing of Environment 121, 236–251.

Guanter, L., Zhang, Y., Jung, M., Joiner, J., Voigt, M., Berry, J. A., Frankenberg, C., Huete, A. R., Zarco-Tejada, P., Lee, J.-E., et al., 2014. Global and time-resolved monitoring of crop photosynthesis with chlorophyll fluorescence. Proceedings of the National Academy of Sciences 111 (14), E1327–E1333.

730 Hall, F. G., Hilker, T., Coops, N. C., Lyapustin, A., Huemmrich, K. F., Mid-
731 dleton, E., Margolis, H., Drolet, G., Black, T. A., 2008. Multi-angle remote
732 sensing of forest light use efficiency by observing pri variation with canopy
733 shadow fraction. Remote Sensing of Environment 112 (7), 3201–3211.

734 Hilker, T., Lyapustin, A., Hall, F. G., Wang, Y., Coops, N. C., Drolet, G.,
735 Black, T. A., 2009. An assessment of photosynthetic light use efficiency from
736 space: Modeling the atmospheric and directional impacts on PRI reflectance.
737 Remote Sensing of Environment 113 (11), 2463–2475.

738 Jacquemoud, S., Baret, F., 1990. PROSPECT: A model of leaf optical properties
739 spectra. Remote Sensing of Environment 34 (2), 75–91.

740 Jacquemoud, S., Verhoef, W., Baret, F., Bacour, C., Zarco-Tejada, P. J., Asner,
741 G. P., François, C., Ustin, S. L., 2009. PROSPECT+ SAIL models: A review
742 of use for vegetation characterization. Remote Sensing of Environment 113,
743 S56–S66.

744 Joiner, J., Guanter, L., Lindstrot, R., Voigt, M., Vasilkov, A., Middleton, E.,
745 Huemmrich, K., Yoshida, Y., Frankenberg, C., 2013. Global monitoring of
746 terrestrial chlorophyll fluorescence from moderate-spectral-resolution near-
747 infrared satellite measurements: methodology, simulations, and application
748 to GOME-2. Atmospheric Measurement Techniques 6 (10), 2803–2823.

749 Joiner, J., Yoshida, Y., Vasilkov, A., Middleton, E., et al., 2011. First obser-
750 vations of global and seasonal terrestrial chlorophyll fluorescence from space.
751 Biogeosciences 8 (3), 637–651.

752 Krause, G., Weis, E., 1991. Chlorophyll fluorescence and photosynthesis: the
753 basics. Annual Review of Plant Biology 42 (1), 313–349.

754 Lee, J.-E., Frankenberg, C., van der Tol, C., Berry, J. A., Guanter, L., Boyce,
755 C. K., Fisher, J. B., Morrow, E., Worden, J. R., Asefi, S., et al., 2013. Forest
756 productivity and water stress in amazonia: observations from gosat chloro-

phyll fluorescence. Proceedings of the Royal Society of London B: Biological Sciences 280 (1761), 20130171.

Lindfors, L., Hölttä, T., Lintunen, A., Porcar-Castell, A., Nikinmaa, E., Juurola, E., 2015. Dynamics of leaf gas exchange, chlorophyll fluorescence and stem diameter changes during freezing and thawing of scots pine seedlings. Tree Physiology, 1–11.

Maxwell, K., Johnson, G. N., 2000. Chlorophyll fluorescence —a practical guide. Journal of Experimental Botany 51 (345), 659–668.

Meroni, M., Busetto, L., Colombo, R., Guanter, L., Moreno, J., Verhoef, W., 2010. Performance of spectral fitting methods for vegetation fluorescence quantification. Remote Sensing of Environment 114 (2), 363–374.

Meroni, M., Picchi, V., Rossini, M., Cogliati, S., Panigada, C., Nali, C., Lorenzini, G., Colombo, R., 2008a. Leaf level early assessment of ozone injuries by passive fluorescence and photochemical reflectance index. International Journal of Remote Sensing 29 (17-18), 5409–5422.

Meroni, M., Rossini, M., Guanter, L., Alonso, L., Rascher, U., Colombo, R., Moreno, J., 2009. Remote sensing of solar-induced chlorophyll fluorescence: Review of methods and applications. Remote Sensing of Environment 113 (10), 2037–2051.

Meroni, M., Rossini, M., Picchi, V., Panigada, C., Cogliati, S., Nali, C., Colombo, R., 2008b. Assessing steady-state fluorescence and PRI from hyperspectral proximal sensing as early indicators of plant stress: The case of ozone exposure. Sensors 8 (3), 1740–1754.

Müller, N., 1874. Beziehungen zwischen assimilation, absorption und fluoreszenz im chlorophyll des lebenden blattes. Jahrbuch des Wissenschaftlicher Botanik 9, 42–49.

783 Plascyk, J. A., 1975. The MK II Fraunhofer line discriminator (FLD-ii) for
784 airborne and orbital remote sensing of solar-stimulated luminescence. Optical
785 Engineering 14 (4), 339–346.

786 Porcar-Castell, A., Tyystjärvi, E., Atherton, J., van der Tol, C., Flexas, J.,
787 Pfündel, E. E., Moreno, J., Frankenberg, C., Berry, J. A., 2014. Linking
788 chlorophyll a fluorescence to photosynthesis for remote sensing applications:
789 mechanisms and challenges. Journal of Experimental Botany 65, 4065–4095.

790 Rascher, U., Alonso, L., Burkart, A., Cilia, C., Cogliati, S., Colombo, R., Damm,
791 A., Drusch, M., Guanter, L., Hanus, J., et al., 2015. Sun-induced fluorescence-
792 a new probe of photosynthesis: First maps from the imaging spectrometer
793 HyPlant. Global Change Biology 21, 4673–4684.

794 Rossini, M., Meroni, M., Migliavacca, M., Manca, G., Cogliati, S., Busetto, L.,
795 Picchi, V., Cescatti, A., Seufert, G., Colombo, R., 2010. High resolution field
796 spectroscopy measurements for estimating gross ecosystem production in a
797 rice field. Agricultural and Forest Meteorology 150 (9), 1283–1296.

798 Rossini, M., Nedbal, L., Guanter, L., Ač, A., Alonso, L., Burkart, A., Cogliati,
799 S., Colombo, R., Damm, A., Drusch, M., et al., 2015. Red and far red sun-
800 induced chlorophyll fluorescence as a measure of plant photosynthesis. Geo-
801 physical Research Letters 42 (6), 1632–1639.

802 Van der Tol, C., Berry, J., Campbell, P., Rascher, U., 2014. Models of fluo-
803 rescence and photosynthesis for interpreting measurements of solar-induced
804 chlorophyll fluorescence. Journal of Geophysical Research: Biogeosciences
805 119 (12), 2312–2327.

806 Van der Tol, C., Verhoef, W., Timmermans, J., Verhoef, A., Su, Z., 2009. An in-
807 tegrated model of soil-canopy spectral radiances, photosynthesis, fluorescence,
808 temperature and energy balance. Biogeosciences 6 (12), 3109–3129.

809 Verhoef, W., 1984. Light scattering by leaf layers with application to canopy

reflectance modeling: the SAIL model. Remote Sensing of Environment 16 (2), 125–141.

Verhoef, W., 1998. Theory of radiative transfer models applied in optical remote sensing of vegetation canopies. Ph.D. thesis, Wageningen Agricultural University.

Verhoef, W., 2011. Modeling vegetation fluorescence observations. In: Proceedings of the EARSel 7th SIG-Imaging Spectroscopy Workshop, Edinburgh, UK. pp. 11–13.

Verhoef, W., van der Tol, C., Middleton, E., 2014. Vegetation canopy fluorescence and reflectance retrieval by model inversion using optimization. In: 5th International Workshop on Remote Sensing of Vegetation Fluorescence, Paris, France. Vol. 2224.

Verrelst, J., Rivera, J. P., van der Tol, C., Magnani, F., Mohammed, G., Moreno, J., 2015. Global sensitivity analysis of the scope model: What drives simulated canopy-leaving sun-induced fluorescence? Remote Sensing of Environment 166, 8–21.

Vilfan, N., Van der Tol, C., Muller, O., Rascher, U., Verhoef, W., submitted. A model for leaf fluorescence, reflectance and transmittance spectra: Fluspect. Remote Sensing of Environment —, —.

Wang, W.-M., Li, Z.-L., Su, H.-B., 2007. Comparison of leaf angle distribution functions: effects on extinction coefficient and fraction of sunlit foliage. Agricultural and Forest Meteorology 143 (1), 106–122.

Weis, E., Berry, J. A., 1987. Quantum efficiency of photosystem ii in relation to energy-dependent quenching of chlorophyll fluorescence. Biochimica et Biophysica Acta (BBA) - Bioenergetics 894 (2), 198 – 208.

Wullschleger, S. D., 1993. Biochemical limitations to carbon assimilation in C3 plants – A retrospective analysis of the a/ci curves from 109 species. Journal of Experimental Botany 44 (5), 907–920.

838 Zarco-Tejada, P. J., González-Dugo, V., Berni, J. A., 2012. Fluorescence, tem-
839 perature and narrow-band indices acquired from a UAV platform for water
840 stress detection using a micro-hyperspectral imager and a thermal camera.
841 Remote Sensing of Environment 117, 322–337.

842 Zarco-Tejada, P. J., Morales, A., Testi, L., Villalobos, F., 2013. Spatio-temporal
843 patterns of chlorophyll fluorescence and physiological and structural indices
844 acquired from hyperspectral imagery as compared with carbon fluxes mea-
845 sured with eddy covariance. Remote Sensing of Environment 133, 102–115.

846 Zhang, Y., Guanter, L., Berry, J. A., Joiner, J., Van der Tol, C., Huete, A.,
847 Gitelson, A., Voigt, M., Köhler, P., 2014. Estimation of vegetation photosyn-
848 thetic capacity from space-based measurements of chlorophyll fluorescence for
849 terrestrial biosphere models. Global Change Biology 20 (12), 3727–3742.